Tectonophysics 738–739 (2018) 112–123

Contents lists available at ScienceDirect

Tectonophysics

journal homepage: www.elsevier.com/locate/tecto

Temporal slip-rate stability and variations on the Hope Fault, New Zealand, during the late Quaternary

Narges Khajavi[a,*], Andrew Nicol[a], Mark C. Quigley[b], Robert M. Langridge[c]

[a] Department of Geological Sciences, University of Canterbury, New Zealand
[b] School of Earth Sciences, University of Melbourne, Australia
[c] GNS Science, Lower Hutt, Wellington, New Zealand

ARTICLE INFO

Keywords:
Hope Fault
LiDAR
Slip variability
Slip rate
Dextral strike slip

ABSTRACT

The Hope Fault transfers slip from Hikurangi subduction to the Alpine Fault in the northern South Island of New Zealand. It accommodates mainly dextral strike slip and currently carries the highest slip rate in the Marlborough Fault System. Displacements, displacement rates and earthquake recurrence intervals have been determined using a combination of high resolution LiDAR for 59 dextral displacements (~2.5–200 m) together with calibrated radiocarbon ages (~130 yr to 13,000 yr) for abandoned stream channels, terrace risers and alluvial fans. Mean single-event displacement (SED) of 3 ± 0.6 m (2.2 to 4.6 m for 21 measurements) and mean recurrence interval of ~266 ± 100 yr (range 128 to 560 yr) have been determined for the five most recent surface-rupturing earthquakes. On time scales ≥2300 yr the dextral slip rate is uniform at 12.2 ± 2.4 mm/yr, however, when averaged over time intervals of ~230 to 1700 yr slip rates range from ~4 to 46.4 mm/yr. This order-of-magnitude variability in slip rate over shorter timescales cannot be fully attributed to errors in displacement and age data, and is at least partly due to variations in earthquake recurrence interval and inferred SED. Short-term non-characteristic earthquake behaviour may be due to changes in fault loading arising from stress interactions between different segments of the Hope Fault and nearby faults.

1. Introduction

Seismic hazard parameters for faults capable of surface-rupturing earthquakes are often evaluated by determining the displacement and age of geomorphic markers (Weldon and Sieh, 1985; Langridge and Berryman, 2005; Khajavi et al., 2014; Zielke et al., 2015), and by paleoseismologic trenching of displaced stratigraphy (Scharer et al., 2007; Langridge et al., 2013; Hornblow et al., 2014; Khajavi et al., 2016). Such studies often reveal discrepancies in slip rates calculated over shorter (e.g., $< 10^3$–10^4 yr) and longer (e.g., 10^3–10^5 yr) timescales (e.g., Weldon et al., 2004; Nicol et al., 2009; Ninis et al., 2013; Rittase et al., 2014). Temporal changes in slip rates have been attributed to a number of factors including: (1) uncertainties on the displacements and their ages, (2) incomplete sampling of wide deformation zones or long seismic cycles, (3) temporal and spatial changes in strain rates, and (4) changes in fault slip vectors (Cowie and Roberts, 2001; Polonia et al., 2004; Oskin et al., 2008; Cowie et al., 2012; Dolan and Haravitch, 2014). For example, paleoseismic trenches often provide short (10^2–10^4 yr) or incomplete records of seismic activity due to their limited depths and lateral extent, uncertainties in the dating of earthquakes, and complex faulting especially where strike-slip faults traverse laterally heterogeneous units (Hartleb et al., 2003, 2006; Mason et al., 2006; Scharer et al., 2007; Cowie et al., 2012; Quigley et al., 2012; Langridge et al., 2013; Ninis et al., 2013; Hornblow et al., 2014; Khajavi et al., 2016). Despite recognition that late Quaternary slip rates can be variable, questions remain as to how common such variability is and what geological processes produce it.

In the study, we measure displacements along the Hope Fault using airborne light detection and ranging (LiDAR) data and previously published radiocarbon ages of the faulted geomorphic features to examine the stability of slip rates on the Hurunui segment of the Hope Fault, New Zealand (Fig. 1). Fifty-nine new strike-slip displacements ranging from ~2.5 to 200 m with scarp heights of ~0.1 to 22 m are obtained and combined with radiocarbon dates (Langridge and Berryman, 2005; Langridge et al., 2013; Khajavi et al., 2016) to constrain fault strike-slip rates over time intervals of ~230–13,000 yr at four localities along the Hurunui segment. The variability of single-event displacement for individual earthquakes is examined by analysing cumulative displacements, while the timing of distinct earthquakes is constrained by prior trenching data combined with

* Corresponding author.
E-mail address: narges.amir.nz@gmail.com (N. Khajavi).

https://doi.org/10.1016/j.tecto.2018.05.001
Received 2 October 2017; Received in revised form 1 May 2018; Accepted 2 May 2018
Available online 05 May 2018
0040-1951/

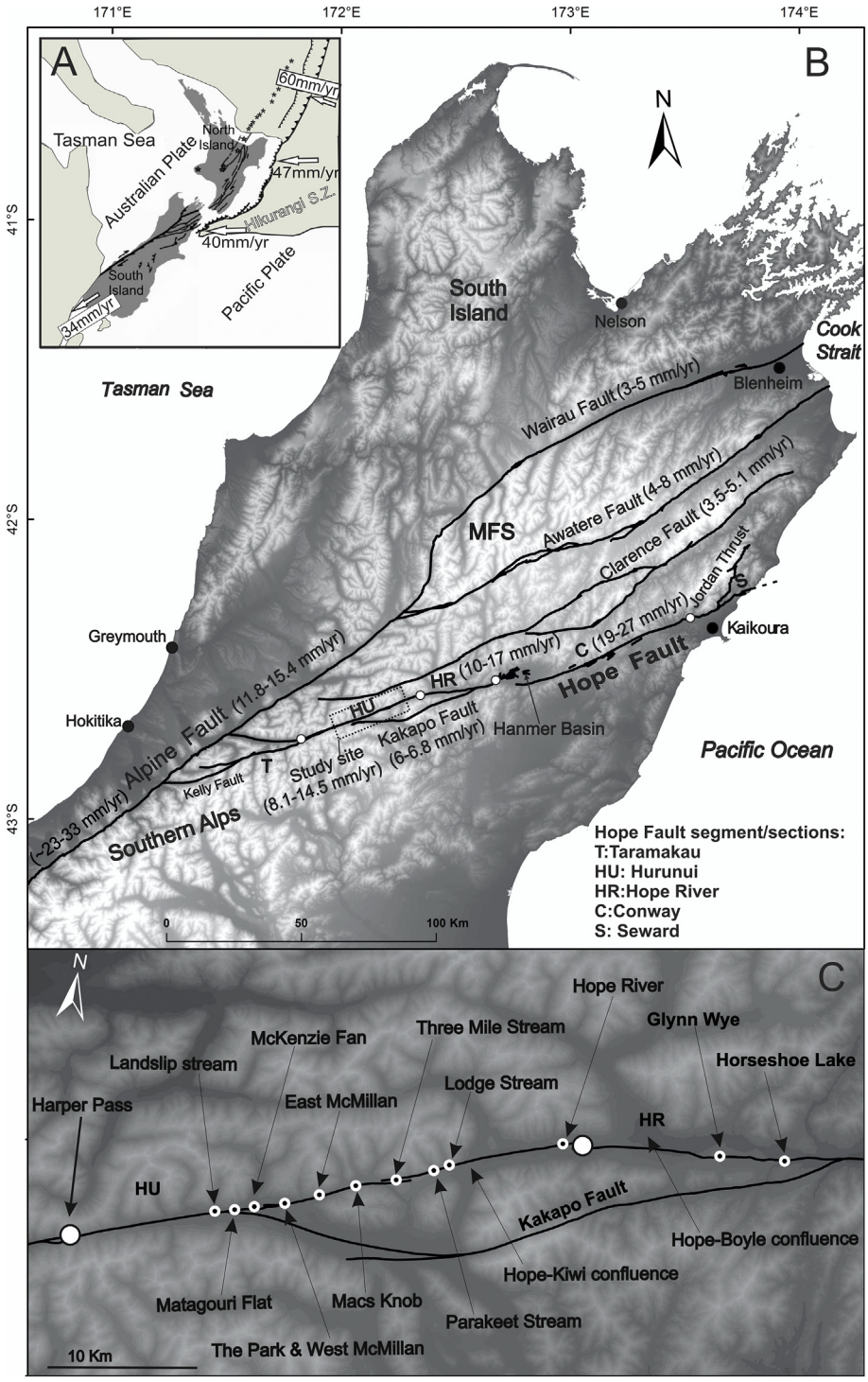

Fig. 1. Tectonic setting of New Zealand and the Marlborough Fault System (MFS) in the northern South Island. Background is a 25 m DEM. (A), New Zealand plate boundary including subduction zones and major faults. Nuvel-1 plate rates (mm/yr) and orientations are after DeMets et al. (1994). (B), Digital elevation model of the northern South Island including the MFS and Alpine Fault is shown. The late Pleistocene-Holocene slip rate estimates (values in brackets) for the Hurunui, Hope River and Conway segments/sections are presented in mm/yr (Cowan, 1990; Cowan and McGlone, 1991; Yang, 1991; Langridge et al., 2003; Langridge and Berryman, 2005). The late Pleistocene-Holocene slip rate estimates for other faults within the MFS, at the junction of the Hope Fault with the Alpine Fault, and for south of the junction of the Hope and Alpine faults are also presented (Norris and Cooper, 2001; Mason et al., 2006; Zachariasen et al., 2006; Van Dissen and Nicol, 2009; Langridge et al., 2010). Segment/section boundaries are marked by circles. (C), Site names and locations along the study area are shown. Earthquake age data used in this study are from the Hope River site (Khajavi et al., 2016). Slip rate data along the Hope River segment are from Glynn Wye and Horseshoe lake sites (Cowan, 1990; Cowan and McGlone, 1991). Surface age data used in this study come from Matagouri Flat, McKenzie Stream, Macs Knob, Hope-Kiwi confluence and Hope River sites (see Table 2).

radiocarbon and optically stimulated luminescence (OSL) dating, dendrochronology, and OxCal modelling (Khajavi et al., 2016). The variability of slip rates over different timescales and the potential factors causing these changes are investigated and discussed.

2. Tectonic setting, geology and kinematics

The Hope Fault is part of the Marlborough Fault System (MFS) in the northern South Island of New Zealand, which links the Hikurangi subduction zone to the Alpine Fault in the south (Van Dissen and Yeats, 1991; Berryman et al., 1992; Nicol and Van Dissen, 2002) (Fig. 1). The MFS comprises four major dextral strike-slip faults: the Wairau, Awatere, Clarence, and Hope faults with total strike-slip rates across the system of ~39–48 mm/yr (Lensen, 1962; Berryman and Beanland, 1991; Van Dissen and Yeats, 1991; Knuepfer, 1992; DeMets et al., 1994, 2010; Beavan et al., 2002; Wallace et al., 2007, 2012). The ENE-striking Hope Fault (~230 km long) is the youngest and southernmost fault in the MFS (Freund, 1971; Van Dissen, 1989; Cowan, 1990; Wood et al., 1994; Langridge and Berryman, 2005). The Hope Fault accommodated late Quaternary slip rates of ~10–30 mm/yr and is the second fastest moving fault in New Zealand after the Alpine Fault (Cowan, 1989, 1990; Cowan and McGlone, 1991; Van Dissen and Yeats, 1991; Knuepfer, 1992; Langridge et al., 2003; Langridge and Berryman, 2005) (Fig. 1). Field, aerial photography, and LiDAR mapping indicate that

the Hope Fault comprises five segments (from west to east: Taramakau, Hurunui, Hope River, Conway, and Seaward) of ~20 to 70 km length defined by fault-trace geometries and slip rates (Fig. 1) (McKay, 1890; Freund, 1971; Cowan, 1989; Langridge et al., 2003; Langridge and Berryman, 2005; Langridge et al., 2013; Beauprêtre et al., 2012; Khajavi et al., 2014). The Hope Fault is a major source of seismic hazard and last ruptured in the Mw 7.1 ± 0.1 1888 Amuri earthquake with a surface-trace length of 44–70 km (McKay, 1890; Khajavi et al., 2016).

The Hurunui segment of the Hope Fault is ~42 km long (Langridge et al., 2013) (Fig. 1), strikes at 070°–075° (approximately parallel to the relative Pacific-Australian plate motion vector) and dips ~85° NW (Khajavi et al., 2014, 2016). At a regional scale, this segment of the fault is remarkably straight with no major step-overs or bends and is approximately parallel to the relative plate motion vector, making it optimally oriented for strike-slip motion (see Khajavi et al., 2014). Dextral displacements along the main fault trace (MFT) are well preserved (Langridge and Berryman, 2005). Khajavi et al. (2016) excavated paleoseismic trenches and identified six earthquakes at 1888 (historical), and 110–210, 471–327, 858–1131, 1399–1511, and 1531–1577 (cal. yr B.P.) indicating a mean recurrence interval of ~298 ± 88 yr with inter-event times ranging from 98 to 595 yr. They concluded that the large variance in inter-event times could be due to incomplete sampling and/or variations in rupture lengths or locations close to the boundary between the Hope River and Hurunui segments.

Previous studies have examined geomorphic slip rates of the Hope Fault from three sites along the Hurunui segment, two sites along the Hope River segment, and four sites along the Conway segment using cumulative slip measurements and ages of faulted landforms (Clayton, 1965, 1968; Freund, 1971; Suggate, 1965; Suggate et al., 1978; Hardy and Wellman, 1984; Wellman, 1985; Knuepfer, 1984, 1988; Cowan, 1989, 1990; Van Dissen, 1989; Cowan and McGlone, 1991; McMorran, 1991; Van Dissen and Yeats, 1991; Langridge et al., 2003; Langridge and Berryman, 2005; Khajavi, 2015; Khajavi et al., 2016). Slip rate estimates averaged for the late Quaternary on the Hurunui, Hope River, and Conway segments are 8.1–14.5 mm/yr, 10–17 mm/yr, and 23 ± 4 mm/yr, respectively (Cowan, 1990; Cowan and McGlone, 1991; Langridge et al., 2003; Langridge and Berryman, 2005) (Table 1). Geodetic data (GPS) indicate decadal slip rates of 13.9 mm/yr, 15.5–16.7 mm/yr, and 18.4 mm/yr for the Hurunui, Hope River and Conway segments of the fault, respectively (Wallace et al., 2012) (Table 1). Correlative bedrock lithologies on opposite sides of the Hope Fault have been displaced dextrally by ~8.5 to 40 km (Freund, 1971; Nathan et al., 2002; Rattenbury et al., 2006), which could have accrued in ~0.5–2 Ma if average late Quaternary slip rates also apply throughout the Quaternary.

3. Data and methodology

3.1. Displacement measurements

Horizontal and vertical components of displacements were measured using displaced geomorphic features that were continuous across the fault prior to faulting. Displaced late Quaternary landforms along the Hurunui segment of the Hope Fault were primarily formed following the Last Glacial Maximum (LGM-Otira glaciation; ~28–18 kyr B.P.) (Nathan et al., 2002; Alloway et al., 2007; Barrell and Townsend, 2012). These geomorphic displacement markers include alluvial fans and channels, landslides/debris deposits, terrace risers, gravitational failure scarps, and cut banks/cliffs which were mapped and displacements measured using 2 m and 1 m hillshade models generated from LiDAR (Khajavi et al., 2014; Khajavi, 2015). Some of the fault traces and displaced landforms and/or the existence of the geomorphic features along accessible sites were field-validated. Displacements are measured both for the MFT and fault traces within the wider fault deformation zone (FDZ).

Scarp heights were estimated from topographic profiles

Table 1
A comparison of geomorphic, geodetic and paleoseismic slip rates along the Hope Fault. Abbreviations: SED; single event displacement, and RI; recurrence interval. This study estimates the paleoseismic slip rates using the presented SEDs and RIs from the second column. Abbreviations: H and A are horizontal displacement and age, respectively. See Fig. 1 for site locations.

Segments	Events	Estimated SED (m)	Paleoseismic slip rate (SED/RI) (mm/yr)	Geomorphic slip rate (mm/yr)	Geodetic slip rate (mm/yr)[g]
Hurunui (West)	2 events in the last ~600 yr (RI: ~300 yr) (Matagouri Flat site)[a]	4.5 ± 0.6[a]	15 ± 2	9.5 ± 1.5 (H: 22 ± 2, age: 2331 ± 55) (Mckenzie Fan site)[b] 13 ± 1.5 (H: 166 ± 17, age: 10,782 ± 60) (Macs Knob site)[b]	13.9
Hurunui (East)	6 events in the last ~1700 yr (RI: ~283 yr) (Hope River site)[c]	2.6 ± 0.3 (1 event?) Or 2.6 ± 0.3 (2 events?)	9.2 ± 1 4.6 ± 0.5	8.3 ± 1.8 (H: 14 ± 3, age: ~1700) (Hope River site)[c]	
Hope River (Central)	5 events in the last ~700 yr (RI: ~140 yr) (Horseshoe Lake site)[d, e]	2 ± 0.5	14.3 ± 3.6	10.5 ± 0.5 (H: 36 ± 0.5 m, age: 3336 ± 65) (Horseshoe Lake site)[d]	15.5–16.7
Conway (East)	2 events in the last ~700 yr (RI: ~350 yr) (Glynn Wye site) 3 events in the last ~800 yr (RI: ~267 yr) (Greenburn Stream site)[f]	2 ± 0.5 5.5 ± 0.5	5.7 ± 1.4 20.6 ± 1.9	14 ± 3(H: 230 ± 20 m, age: ~17,000 ± 2000) (Glynn Wye)[e] < 23 ± 4 (H: 115 ± 15, age: 5066 ± 189) (Greenburn Stream site)[f]	18.4

Ages are presented in yr B.P.
[a] Langridge et al. (2013).
[b] Langridge and Berryman (2005).
[c] Khajavi (2015), Khajavi et al. (2016).
[d] Cowan and McGlone (1991).
[e] Cowan (1990).
[f] Langridge et al. (2003).
[g] Wallace et al. (2012).

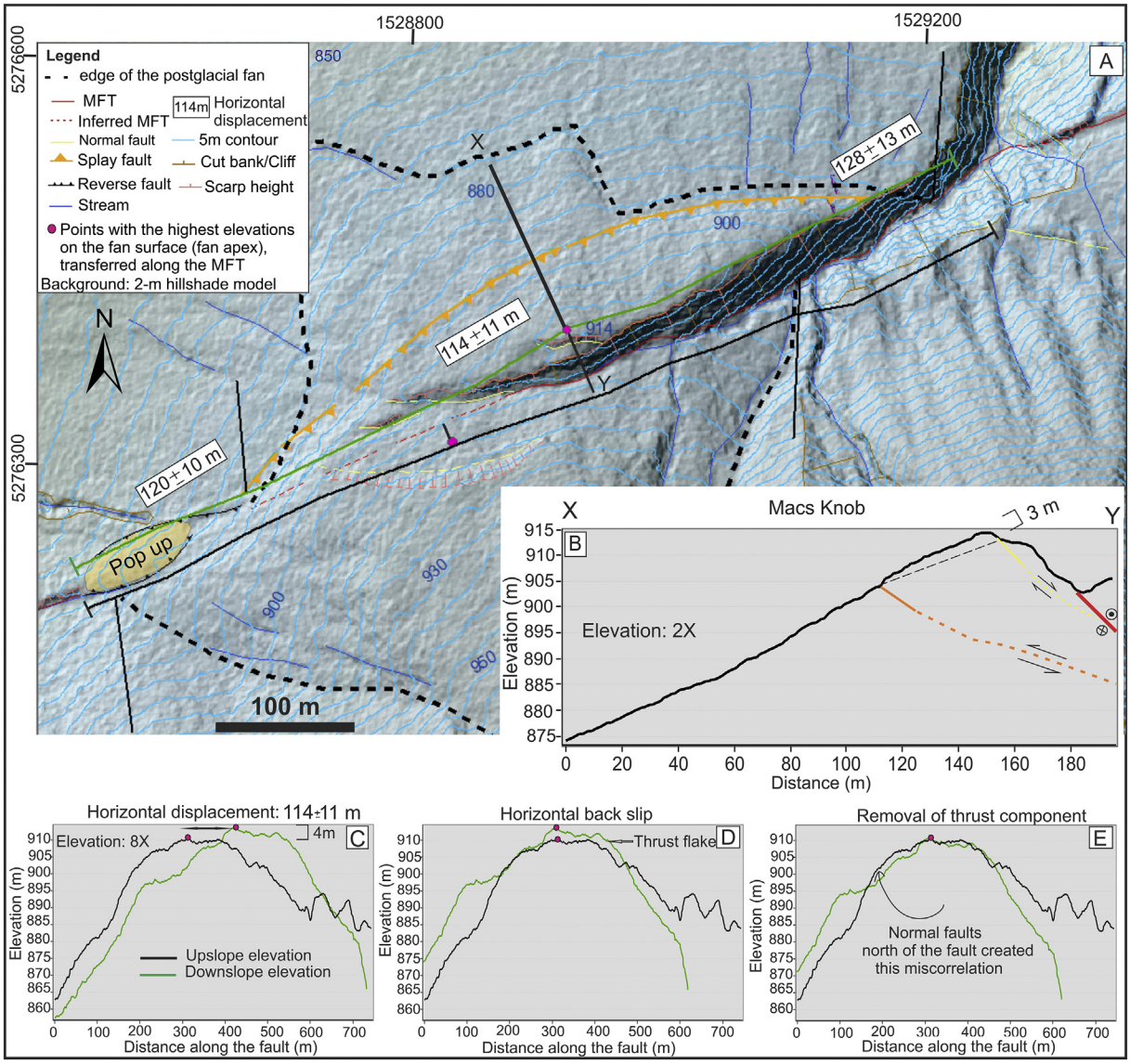

Fig. 2. Macs Knob area near the middle section of the Hurunui segment (see Fig. 1C for location). (A), The largest displaced fan along the Hope Fault. Upslope and downslope elevation profiles (black and green lines) are extended along the fan on both sides of the fault. Profile XY is extended across the thrust flake and the MFT on the fan surface. Horizontal displacements of the fan margins and apex are measured. (B), Cross-section XY shows fault model at depth (fault dips and orientations are used from Khajavi et al. (2014)) and vertical displacement on the thrust flake. (C), Upslope and downslope elevation profiles show the horizontal and vertical displacements of the fan. (D), Back-slipping approach is used to correlate the apex of the fan. Vertical displacement of the thrust flake is shown. (E), Thrust component is removed. Not only the apex, but also the middle section of the fan is now matched.

perpendicular to the trend of the fault trace, which were produced from the LiDAR digital elevation model (DEM) using ArcMap (GIS) software. On the profiles, the vertical separations (i.e., scarp heights) across the fault were measured and measurement uncertainty assigned to scarp heights taking account of the erosion or deposition along the fault scarps.

Previous studies suggest that the vertical displacements along the Hurunui segment are small (H:V ~ 7 ± 2:1) relative to the horizontal displacements (Langridge and Berryman, 2005). In this study, we show that scarp heights are not representative of the actual vertical slip. For example, in the middle section of the Hurunui segment, at the Macs Knob site, a fan has been displaced horizontally by ~120 m producing a maximum scarp height of ~22 m (Fig. 2). A back-slipping approach (e.g., Manighetti et al., 2015; Zielke et al., 2015) was used to reconstruct the original shape of the fan at Macs Knob prior to faulting and to estimate vertical and horizontal displacements of the surface (Fig. 2A, B and C). Back-slipping of the fan between topographic profiles indicate horizontal displacements of 121 ± 11 m for the fan surface (i.e. the mean of the 3 measurements on Fig. 2). By comparison, the estimated vertical displacement of the fan apex is 4 ± 2 m which is significantly smaller than the maximum apparent scarp height (~22 m). These displacements produce a mean H:V ratio of ~33:1, which is significantly higher than ~8:1 estimated assuming that the scarp height is equal to the vertical displacement.

The horizontal displacements were measured using reconstruction of geomorphic markers along the fault strike (Quigley et al., 2012; Rockwell and Klinger, 2013; Zielke et al., 2015). We projected piercing lines to the fault trace along the two sections of a geomorphic feature (i.e., north and south of the fault trace). Subsequently, the horizontal separations between the linear piercing lines along the fault trace were measured on the LiDAR hillshade models. In this method of displacement measurement, uncertainties assigned to displacements are dependent on how well the geomorphic markers are defined, their angular relationship to the fault (smaller angles produce greater uncertainties),

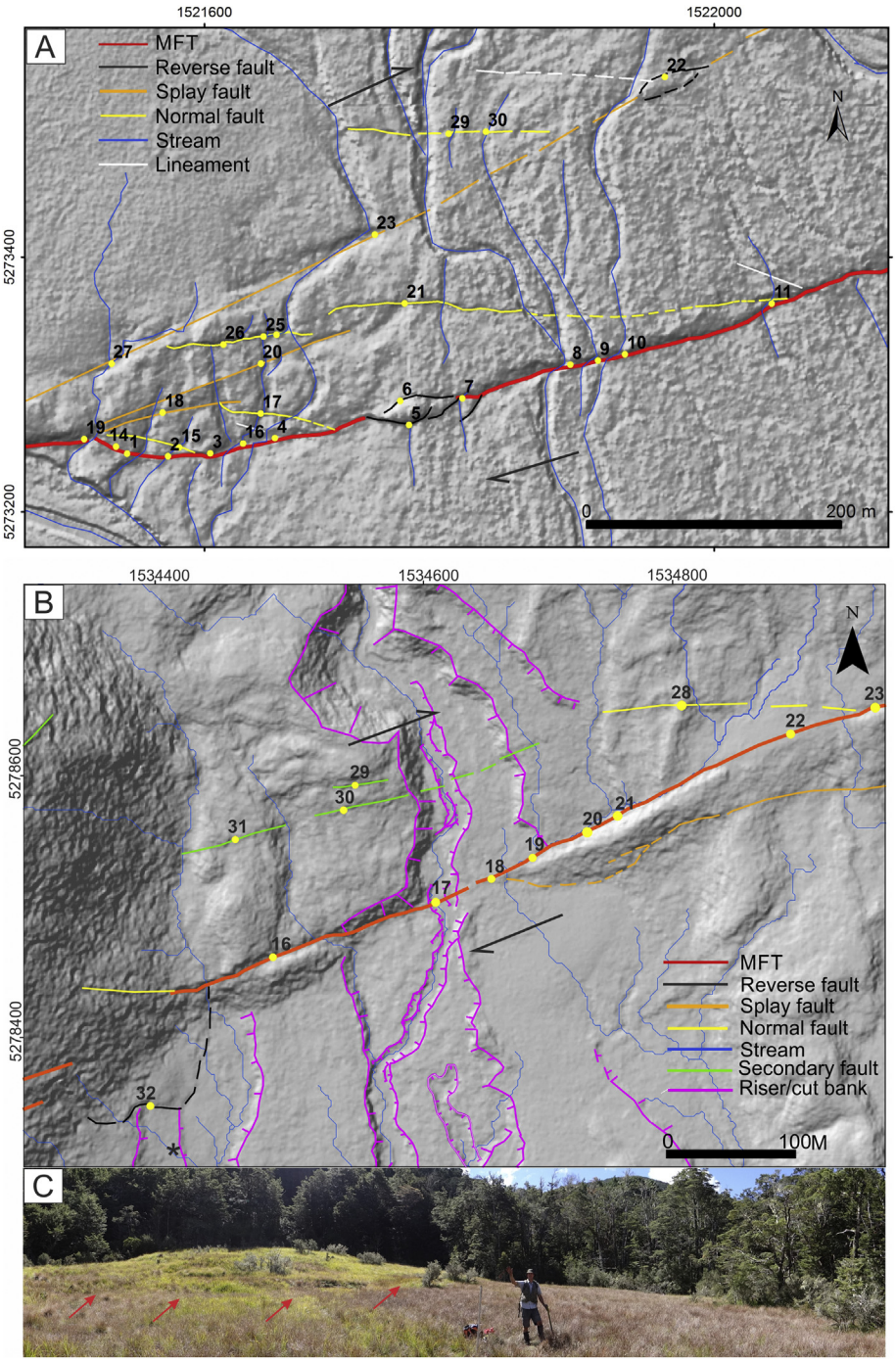

Fig. 3. Fault-trace map of the McKenzie Fan and Parakeet Stream sites including a filed photo from Parakeet site. Background image is a 1 m LiDAR hillshade model. Locations and ID numbers of measured displacements are shown on the map (filled yellow circles). (A), McKenzie Fan site, mapping indicates that some streams have been displaced by multiple fault strands, which define the FDZ. Dextral displacements of such streams (i.e., data points 19 and 27, and data points 16, 17, 20 and 25) have been summed to calculate total slip rate across the FDZ (See Table 3). The age of the fan is 2179–2464 cal. yr B.P. (Table 2 and Langridge and Berryman, 2005). (B), Parakeet Stream site, mapping indicates that Parakeet stream, toe of a debris flow deposits, and channer risers have been displaced. Unlike McKenzie Stream site, it is difficult to identify a feature with multiple displacement along several fault strands. (C), A field photo from Parakeet Stream. Symbol: * on part B, shows the approximate location of the field photo in part C. Arrows point to the reverse fault mapped on part B.

and how far the piercing lines are projected to the fault trace (Rockwell and Klinger, 2013). For this reason, we measured each displaced marker three times using slightly different projections to quantify the internal uncertainties (+/−) resulting from measurement error for displacement measurements. We also estimated the quality of horizontal displacements (McCalpin, 2009; Zielke et al., 2010; Zielke et al., 2012; Scharer et al., 2014; Manighetti et al., 2015) by assigning quality indices (QIs) from 1 to 5 to each measurement (see Table S1 for description of QIs).

More than 400 dextral (n = 160) and vertical (n = 317) displacement measurements (see Tables S1–S3 from the Supplementary file) were collected with only one third of the dextral displacements (n = 59) from the MFT considered to be of sufficient quality for further analysis (i.e., displacements with QIs from 1 to 3 and mean uncertainties/displacement ≤25%, Table S2). Fig. 3A–B shows examples of geomorphic displaced markers and the locations of our measurements at two different sites with small and large displacements. The best estimates of seismic hazard parameters can be achieved when cumulative slip across the entire FDZ is considered. We summed the displacement data collected from the MFT and subsidiary fault traces within the FDZ at the McKenzie Fan site (Fig. 3A) where an individual geomorphic displacement marker was displaced by several fault strands (see Table 3). Apart from McKenzie Fan site, only a few individual geomorphic markers recorded displacements both along the MFT and subsidiary fault strands within the FDZ (see Figs. S1–S4 and Table S3 in the Supplementary file). Most of measurements from FDZ have QIs above 3 because of the quality of the geomorphic markers and the fact that the fault strands within the FDZ are poorly preserved/inferred with

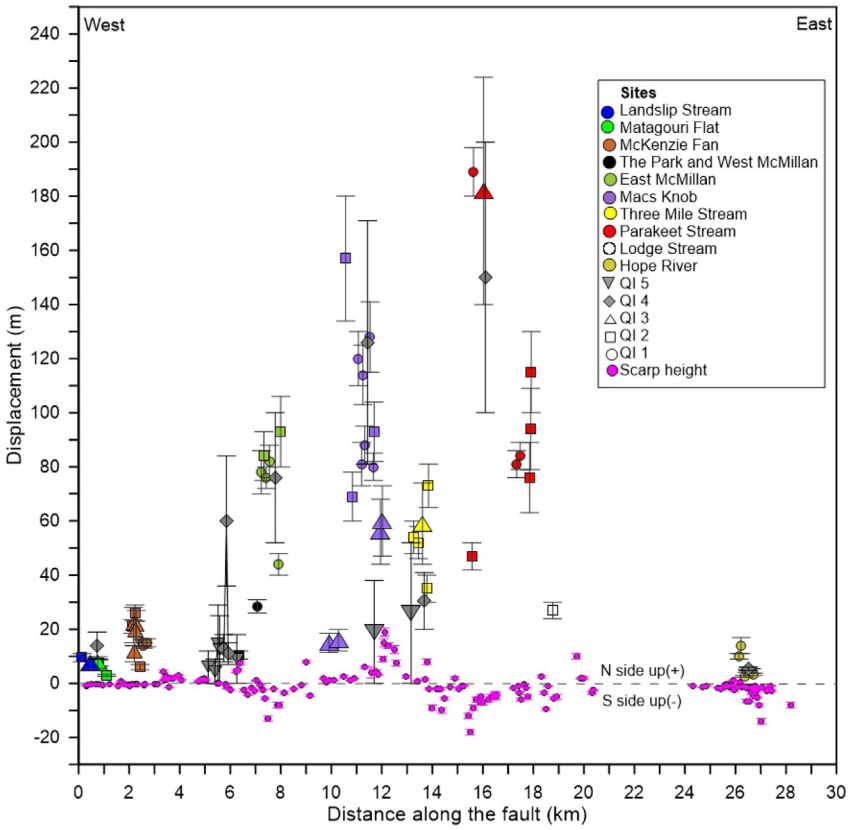

Fig. 4. Dextral displacements and scarp heights distributions along the MFT of the Hurunui segment of the Hope Fault. Dextral displacements are colour-coded according to the sites names (see Fig. 1C for sites locations) and are presented with their QIs. Data with QIs from 4 and 5, which were not used in our analysis, are shown in grey. Note that the displacement data with QIs from 4 to 5 fill a gap on the graph at the Park and West McMillan site.

respect to the MFT (Fig. 3B). Taking that into account, it appears that up to ~50% of deformation might be missing at the sites with such conditions (i.e., The Park and west of McMillan Stream, East of McMillan Stream, Three Mile Stream, Parakeet Stream and Lodge Stream). This does not affect our analysis because we do not have age data for these sites required to examine their slip rates (Table 3).

The spatial distribution of scarp heights and dextral displacements measured from the MFT with QIs of 1 to 5 is shown on Fig. 4, with maximum dextral displacements rising towards the centre of the field area. This distribution of displacements arises because the fault offsets younger landforms towards the eastern and western (Fig. 3A) ends of the mapped fault trace, and does not reflect along-strike changes in fault slip or slip rates. In addition, the plot in Fig. 4 displays scarp heights and supports the view that they are much lower than dextral displacement. Given the high H:V ratios and along strike variations in scarp heights, which may reflect sampling issues and local fault complexities as described above, we focus on dextral slip in this paper.

3.2. Dating displaced landforms

This study utilizes previously published radiocarbon ages from Langridge and Berryman (2005), Langridge et al. (2013) and Khajavi et al. (2016) to constrain the ages of displaced landforms. Radiocarbon samples were obtained from excavated paleoseismic fault trenches, hand-dug pits, and outcrops of deposits younger than the Last Glacial Maximum (LGM). The radiocarbon data used here are summarized in Table 2 and shown on Figs. S1–S4 in the Supplementary file. The existing radiocarbon dates were sampled within ~1.5 m of the ground surface and constrain the ages of geomorphic displacement markers from which slip rates have been estimated. The available ages are presented in cal. yr B.P. and their interpretations are discussed in Table 2. These interpretations have been adopted from the papers which originally presented the radiocarbon dates (Langridge and Berryman, 2005; Langridge et al., 2013; Khajavi et al., 2016).

4. Single event displacement (SED)

To constrain the slip history and characterize variations in SED for the Hurunui segment of the Hope Fault, 21 dextral displacements (with QIs from 1 to 3) of ≤15 m have been plotted in ascending order of size (Fig. 5). For such a plot, steps in the graph are inferred to represent a change in the number of surface rupturing events with more events producing higher displacements (Van Dissen and Nicol, 2009; Nicol et al., 2011). In this paper, we assume that each step represents a single earthquake, although the likelihood that this assumption is correct decreases with increasing age of displaced markers as the uncertainties on the displacements and the time gap between measurements grow. As some displacements have large uncertainties, the steps are displayed by boxes and the line representing the mean displacement. The boxes and mean line define steps in the cumulative displacement with the size of the steps assumed to represent SEDs. To calculate the SED means and their uncertainties, a Monte Carlo procedure was applied to account for the observed displacements of landforms and their uncertainties. The Monte Carlo procedure is similar to that previously employed for quantifying parameters of active faults (e.g., Thompson et al., 2002; Parsons, 2008; Nicol et al., 2016). One thousand displacement measurements were randomly drawn from probability density functions (PDFs) constructed for each of the 21 displacements (Fig. 5A). Each displacement was assumed to be normally distributed about the mean with 2σ uncertainties. The histogram inset (Fig. 5A) displays one output from the analysis and is characterised by five primary modes. The locations and amplitudes of the modes are stable between realisations and define five SEDs. The five red boxes on Fig. 5B are centred on the mean displacement (i.e., blue line) for each mode with the vertical dimension of the rectangle equal to ± 2σ. The Monte Carlo method was also used to calculate the mean SED (i.e., 3 ± 0.6) and its uncertainty using the five individual SEDs as input data.

Based on our analysis, the SED ranges from 2.2 m to 4.6 m (Fig. 5) with a mean of 3 ± 0.6 m. In general, the uncertainties in the slip

Table 2
A summary of the published radiocarbon data by previous studies along the Hurunui segment of the Hope Fault. Ages with * symbol are used to calculate the slip rates in this study. Other ages were estimated to be minimum or maximum according to the previous studies.

Location reference	Sample ID	Lab number	Calibrated age 2σ rage (cal. yr B.P.)	Description
Matagouri Flat Langridge et al. (2013)	MF1E	NZA 18592	515–653*	Plant fragment collected from paleoseismic trench (minimum surface age)
McKenzie Fan Langridge and Berryman (2005)	MKS	NZA13360	2179–2467*	Woody twigs collected from aggradation gravels in McKenzie Stream catchment, 2 km upstream of fault
The Park Langridge and Berryman (2005)	FP	NZA13358	3476–3826	Fresh peat collected from open fissure on the Park (minimum surface age)
Macs Knob (Mc Millan Stream) Langridge and Berryman (2005)	MMS	NZA13361	14,489–15,979	Compact postglacial peat collected from an outcrop including a section of silt and peat sequences northwest of Macs Knob
Macs Knob (Three Mile Stream) Langridge and Berryman (2005)	3MS	NZA13362	6738–7149*	Compact faulted peat collected from a rift zone (fault trough) (minimum surface age)
Hope-Kiwi Lodge Langridge and Berryman (2005)	HKL	NZA13357	12,634–13,060*	Compact postglacial peat collected from an outcrop of postglacial deposit (minimum surface age)
Parakeet Stream Khajavi et al. (2016)	T3W-1	NZA53427	327-490	All peat samples collected from 4 pits on the surfaces of the terrace risers produced by the Parakeet Stream (minimum surface ages)
	T4WP-3	NZA53430	729–794	
	T4EP-4	NZA54174	1399–1525	
	OCWP-6	NZA54154	1900–2105	
Hope River (Hope Shelter) Khajavi et al. (2016)	HS1-19	NZA40317	1418–1688*	Peat sample collected from paleoseismic trench (minimum surface age)

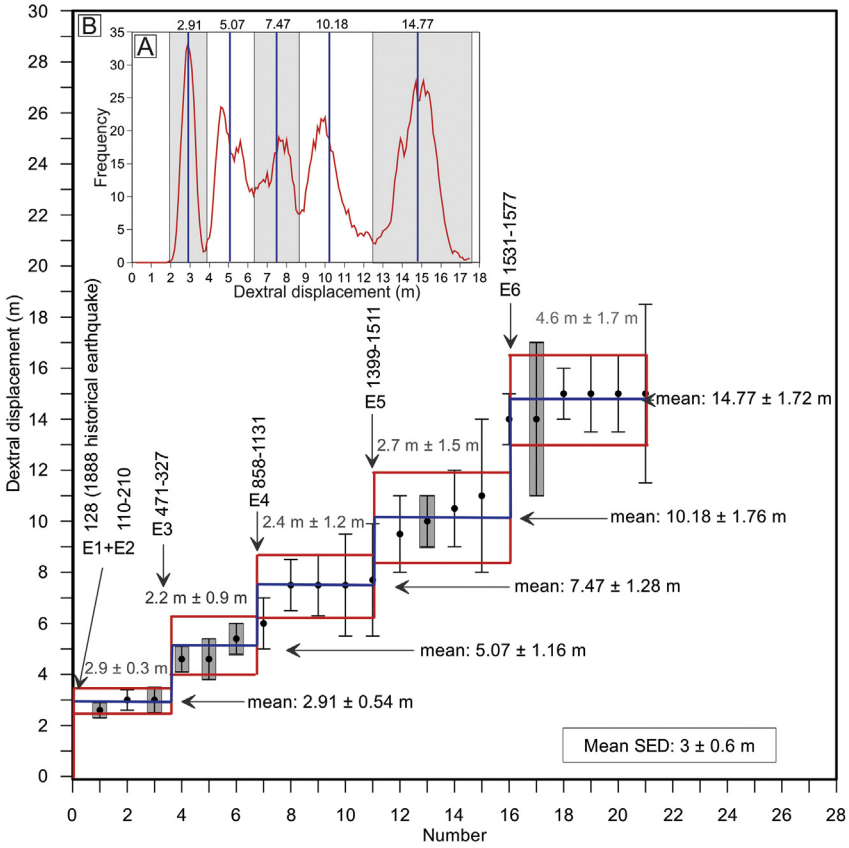

Fig. 5. Frequency distribution and displacement plots for the Hurunui segment. (A), The Monte Carlo statistical method was used to derive frequency distributions of the individual displacements with 2σ uncertainties. (B), The stepped red line shows the number of paleoearthquakes at the vertical segments of the line. Red boxes are drawn based on the frequency distributions of the SEDs. The blue line shows the mean displacement accumulation using the available SED and recurrence data. The Monte Carlo method was used again to calculate the mean SED and its uncertainties. The uncertainty in the mean SED is the standard deviation divided by the square root of the number of SED intervals. Grey numbers represents SEDs per events. The highlighted displacements (in grey) are from the Hope River site (Fig. 1C) and the rest are from other sites within the study area (see Table S3 from Supplementary file). Earthquake ages are presented in yr B.P. and come from paleoseismic trenches excavated at the Hope River site (Khajavi et al., 2016).

measurements increase towards the older events. The SEDs estimated for the four younger events are all in the same range (2.2–2.9 m); however, the SED increases to 4.6 for the oldest event. The rise in SED for the oldest event could be explained by: (1) epistemic error in slip measurements, and/or (2) the oldest SED could represent more than one displacement event. If the second explanation applies, ~6 earthquakes could be required to create ~15 m of slip on the primary fault surface.

5. Slip rates and recurrence intervals

Slip rates are derived from a combination of dextral displacements and dating of displaced landforms. The mean slip-rate of 12.2 ± 2.4 mm/yr has been calculated for all data on the Hurunui segment of the Hope Fault averaged over time intervals of ~ 500–13,000 kyr (Fig. 6). The mean slip rate has been calculated by averaging estimates for sites at Matagouri Flat (13.3 ± 3.2 mm/yr), McKenzie Fan (14.2 ± 3.3 mm/yr and 14.9 ± 3 mm/yr), Macs Knob (9.4 ± 1 mm/yr and 12 ± 1.4 mm/yr), and Hope River

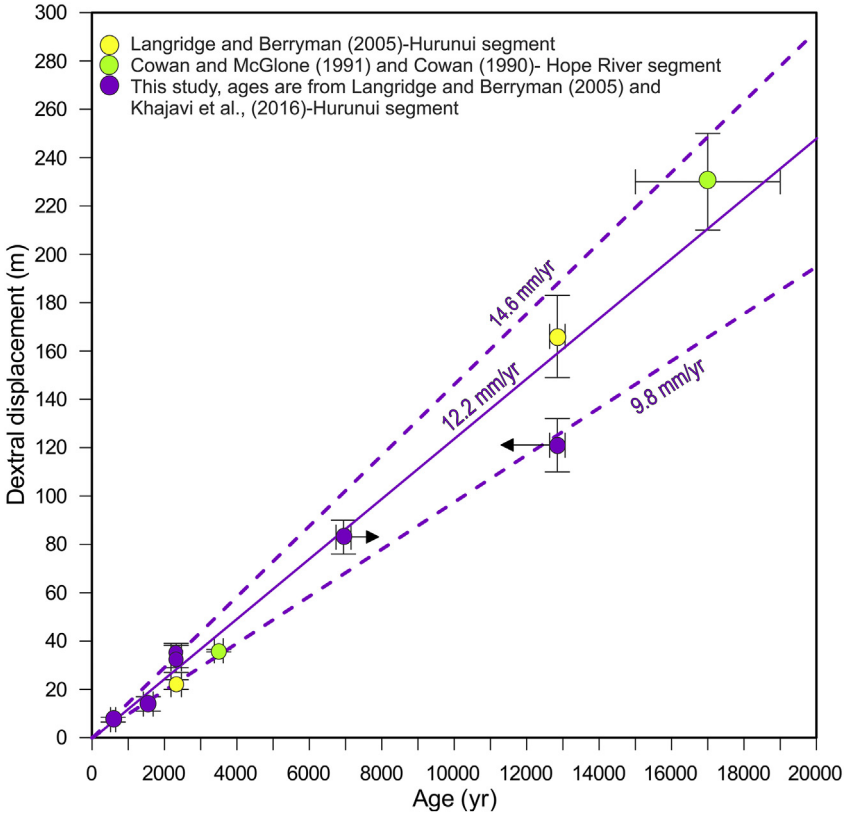

Fig. 6. Slip rate estimates for the Hurunui segment of the Hope Fault. Data from this study (Table 3) are compared to the data from previous studies for the Hurunui and Hope River segments. Black arrows are used where surface ages are estimated to be maximum or minimum (see Table 2). Surface ages are presented in cal. yr B.P.

(9.3 ± 2.7 mm/yr). Consequently, the mean slip rate is not strongly biased by individual displacement measurements or ages from one site. Using these data, three conclusions can be drawn for slip rates on the Hurunui segment of the fault (see Figs. 6–7). These are: (1) slip rates are constant within error when averaged over time intervals of ~2300 to 13,000 yr and longer, (2) slip rate for a given time interval is constant within error along the strike of the Hurunui segment, and (3) slip rates are highly variable since ~1700 yr before present. Slip-rate estimates used to support these results are primarily from the four sites with the best quality cumulative dextral slip and surface ages (Figs. S1–S4 and Tables 3–4). The first-order slip rates derived from these sites compare favourably with the geodetic, paleoseismic and geomorphic slip rates from the previous studies along the Hurunui segment of the Hope Fault (Tables 1 and 3) (e.g., Langridge and Berryman, 2005), while temporal variations in the rates are here explored in detail for the first time.

The mean slip rate from our study is higher than the 9.5 ± 1.5 mm/yr slip rate estimate from Langridge and Berryman (2005) for the McKenzie Fan site. This difference in slip rate principally arises because the LiDAR revealed more fault strands and greater cumulative slip across McKenzie fan than was previously mapped (Figs. 3A and S1C from the Supplementary file). The average slip rate of 14.5 ± 3.2 mm/yr from McKenzie Fan site is the only slip rate along the Hurunui segment that incorporates the entire width of the FDZ and is consistent with the contemporary geodetic slip rate of 13.9 mm/yr (Wallace et al., 2012). Slip rate estimates from paleoseismic trench data along the Hurunui segment (Langridge et al., 2013; Khajavi et al., 2016) are also consistent with our geomorphic slip rate estimates from the same sites (i.e., Matagouri Flat and Hope River sites) (Tables 1 and 3).

The mean slip rate is within the error bounds of slip rates estimated from previous studies on the Hurunui and Hope River segments (yellow and green data points on Fig. 6) (Cowan, 1990; Cowan and McGlone, 1991; Langridge and Berryman, 2005). The slip rates of the McKenzie Fan site (~14.5 ± 3.2 mm/yr) (Table 3 and Fig. 3A) and the Horseshoe Lake site (10.5 ± 0.5 mm/yr) (Table 1) (Fig. 6) are considered to be the best estimates for the Hope and Hurunui segments. Taking this into account, we estimate a mean slip rate of 12.5 ± 2.1 mm/yr for the Hurunui and Hope River segments, which is nearly half of the 23 ± 4 mm/yr slip rate of the Conway segment (Langridge et al., 2003). This change in slip rate may partly reflect the westward transfer of 6.4 ± 0.4 mm/yr (Yang, 1991) from the Hope Fault to the Kakapo Fault (Langridge and Berryman, 2005) (Fig. 1). No slip rate measurements are presently available for the Hope Fault west of the study area where it bifurcates into two main strands and intersects the Alpine Fault. Slip rates on the Alpine Fault increase from 13.6 ± 1.8 mm/yr to ~28 ± 5 mm/yr southwards across junction with the Hope Fault (Norris and Cooper, 2001; Langridge et al., 2010; Nicol et al., 2017), consistent with the Hope Fault system carrying ~10–15 mm/yr to its western termination.

Globally and on the Hope Fault, slip rates vary temporally with changes in the sample duration (Fig. 7) (e.g., Weldon et al., 2004; Mouslopoulou et al., 2009; Nicol et al., 2009). On the Hurunui segment of the Hope Fault, calculated slip rates averaged over time intervals of ~230–1700 yr range by an order of magnitude from 4 (+0.75, −0.55) mm/yr to 46.4 (+23.8, −11.9) mm/yr (Fig. 7). The observed range of slip rates will be partly influenced by errors on the measured displacements and ages (particularly over short sample intervals, e.g., < 500 yr), which are quoted at the 2σ level. The upper limit of the range, which is greater than the plate rate, is defined by one time interval and carries particularly large uncertainties. For these reasons we infer that 46.4 mm/yr is probably greater than the maximum possible slip rate on the fault. If we exclude the displacement and age data used to calculate the 46.4 mm/yr slip rate, a value of ~25 (+3.4, −3.2) mm/yr is required to accommodate the available displacement data between ~1500 and 2300 yr (see dashed line on Fig. 7). Such a rate (~25 mm/yr) is about a factor of 6 higher than the lowest rates on the fault and is consistent with the suggestion that slip rates are highly variable.

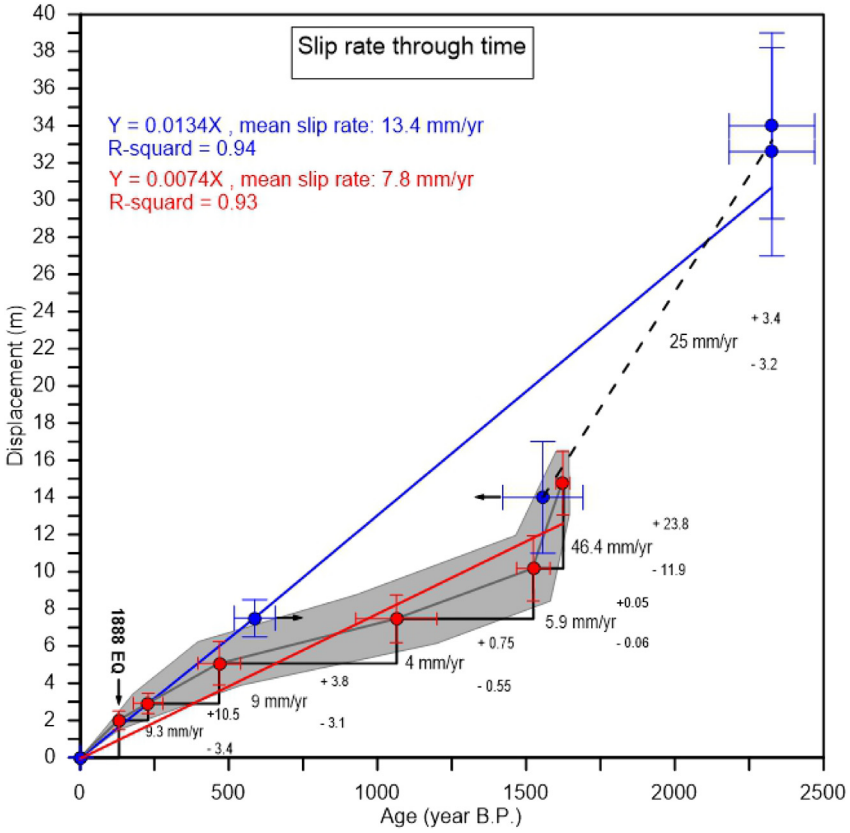

Fig. 7. Displacement-time profile (data in red) is produced for 6 earthquakes over ~1700 yr for the Hurunui segment. Earthquake elapsed times (Khajavi et al., 2016) and mean cumulative displacements from Fig. 5 were used to produce this graph. The mean SED of 2 ± 0.5 (McKay, 1890) was used for the historical 1888 earthquake. Individual slip rates between events are shown with their uncertainties. Cumulative displacements and their surface ages (Table 2) from Matagouri Flat, McKenzie and Hope River sites (data in blue) are also added to the graph to show the slip variability over a slightly larger period of time (i.e., ≤ 2300 yr). Black arrows are used where surface ages are estimated to be minimum or maximum (see Table 2).

Table 3
Slip rate estimates from different sites along the Hurunui segment of the Hope Fault. Sites with available age data are bolded.

Sites	Cumulative dextral displacement (m)	Uncertainty (m)	Min age (cal. yr B.P.)	Max age (cal. yr B.P.)	Min slip rate (mm/yr)	Max slip rate (mm/yr)	Average slip rate (mm/yr)	Uncertainty (mm/yr)
Landslip Stream	9.5	1.5	No data	No data	No data	No data	No data	No data
Matagouri Flat[a]	7.5	1	515	653	10	16.5	13.3	3.2
McKenzie Fan[b]	32.6	5.6	2179	2467	10.9	17.5	14.2	3.3
McKenzie Fan[c]	34	5	2179	2467	11.8	17.9	14.9	3
The Park and West of McMillan Stream	28.5	2.5	No data	No data	No data	No data	No data	No data
East of McMillan Stream	107	15	No data	No data	No data	No data	No data	No data
Macs Knob[d]	121	11	12,634	13,060	8.4	10.4	9.4	1
Macs Knob[e]	83	7	6738	7149	10.6	13.4	12	1.4
Three Mile Stream	73	8	No data	No data	No data	No data	No data	No data
Parakeet Stream	81	5	No data	No data	No data	No data	No data	No data
Parakeet Stream	189	9	No data	No data	No data	No data	No data	No data
Lodge Stream	27	3	No data	No data	No data	No data	No data	No data
Hope River[f]	14	3	1418	1688	6.5	12	9.3	2.7

[a] Surface age from Langridge et al. (2013) was used. Slip value of data point 4 (from Fig. S1B) was used as the best estimate. This yields a maximum slip rate using a minimum surface age. This slip rate incorporates slip along most of the entire fault deformation zone.

[b] Surface age from Langridge and Berryman (2005) was used. Slip values of data points 16, 17, 20 and 25 (see Fig. 4) were summed and used as cumulative slip. This slip rate incorporates slip along the entire fault deformation zone.

[c] Surface age from Langridge and Berryman (2005) was used. Slip values of data points 19 and 27 (see Fig. 4) were summed and used as cumulative slip. This slip rate incorporates slip along the entire fault deformation zone.

[d] Surface age from Langridge and Berryman (2005) near the Hope-Kiwi confluence was used. They also used this age when estimated a slip rate for Macs Knob site. However, this age seems to be old as the fans in Macs Knob area must be post LGM features. The mean slip value of data points 16, 36, and 37 from Fig. S3A which show displacements along fan margins and apex was used. This probably yields a minimum slip rate.

[e] Surface age from Langridge and Berryman (2005) (the younger age presented at the Macs Knob) was used. The mean slip value of data points 25, 26 and 30 from Fig. S3A which show displacements along the middle and margins of the fan was used. This yields a maximum slip rate.

[f] Surface age from Khajavi et al. (2016) was used. This yields a maximum slip rate.

Table 4
Estimates of recurrence intervals from different sites along the Hurunui segment of the Hope Fault. Abbreviation: NoE: number of events. The mean RI ranges are estimated using the SEDs of 3 ± 0.6 m and 2.4 ± 0.2 m; the latter SED is estimated assuming that the displacement of ~ 14.8 m (Fig. 5) includes six earthquakes.

No	Site name	Cumulative slip	NoE (SED: 3 ± 0.6)	Age (cal. yr B.P.)	Slip rate (mm/yr)	RI (SED/slip rate) (yr)	RI (age/NoE) (yr)
1	Matagouri Flat	7.5 ± 1	2–4	515–653	13.3 ± 3.2	145–356	128–327
2	McKenzie Fan	32.6 ± 5.6	8–16	2179–2467	14.2 ± 3.3	137–330	136–308
3	McKenzie Fan	34 ± 5	8–16	2179–2467	14.9 ± 3	134–303	136–308
4	Macs Knob	121 ± 11	31–55	12,634–13,060	9.4 ± 1	231–428	230–421
5	Macs Knob	83 ± 7	21–38	6738–7149	12 ± 1.4	179–340	177–340
6	Hope River	14 ± 3	3–7	1418–1688	9.3 ± 2.7	200–545	203–563
Mean RI range using the mean slip rate of 12.2 ± 2.4 and mean SED of 3 ± 0.6: ~ 164–367 yr							

No	Site name	Cumulative slip	NoE (SED: 2.4 ± 0.2)	Age (cal. yr B.P.)	Slip rate (mm/yr)	RI (SED/slip rate) (yr)	RI (age/NoE) (yr)
1	Matagouri Flat	7.5 ± 1	3–4	515–653	13.3 ± 3.2	133–257	129–218
2	McKenzie Fan	32.6 ± 5.6	10–17	2179–2467	14.2 ± 3.3	126–239	128–247
3	McKenzie Fan	34 ± 5	11–18	2179–2467	14.9 ± 3	123–218	121–224
4	Macs Knob	121 ± 11	42–60	12,634–13,060	9.4 ± 1	212–310	211–311
5	Macs Knob	83 ± 7	29–41	6738–7149	12 ± 1.4	164–245	164–247
6	Hope River	14 ± 3	4–8	1418–1688	9.3 ± 2.7	183–394	177–422
Mean RI range using the mean slip rate of 12.2 ± 2.4 and mean SED of 2.4 ± 0.2: ~151–265 yr							

Inspection of Fig. 7 supports the notion that not all of the variability can be attributed to uncertainties, and we believe that the variable slip rates are also due to temporal changes in earthquake SED and inter-event times or recurrence intervals (RIs) at the ground surface.

RI is known to vary on New Zealand active faults (e.g., Nicol et al., 2006, 2009, 2016) and these changes could have a significant influence on slip rates. In this study, RI estimates for the Hurunui segment of the Hope Fault over the last ~13,000 yr vary between 128 and 560 yr with a mean of ~266 ± 100 yr (Table 4). The estimated range of RI here is comparable to the ~98–595 yr (mean: 298 ± 88 yr) of Khajavi et al. (2016), which was calculated for 1700 yr, but is larger than the range in RI of 310–490 yr (mean: 400 ± 90 yr) estimated by Langridge and Berryman (2005) over the last ~2300 yr. One possible explanation for these differences in RI is that the longer duration samples are incomplete (i.e. it is missing an event or events). If sample incompleteness influences RI and SED variations equally, then the available data suggests that RI is about twice as variable as SED and, if there is no relationship between SED and inter-event times, may have about double the impact on slip rates. For example, RI and SED for the available data (i.e. not corrected for sample incompleteness) vary by up to factors of 4 and 2, respectively, consistent with other faults in New Zealand (Nicol et al., 2006, 2009, 2016) and overseas (Mouslopoulou et al., 2009). Using the observed variability of RI and SED, slip rates of ~4 to 46.4 mm/yr (i.e., minimum rate 2.2 m/0.5 kyr and maximum 4.6 m/0.1 kyr) can be calculated which is similar to the observed range of rates and supports the view that variations in earthquake parameters are key for slip-rate variations. In comparison, if the SED of ~4.6 m records two earthquake events (each ~2.3 m of slip) (Fig. 5), then slip rates of ~4 to 23 mm/yr (i.e., minimum rate 2.2 m/0.5 kyr and maximum 2.3 m/0.1 kyr) and RI of 208 ± 57 yr (range 120 to 420 yr) (Table 4) are calculated. RI and SED for the such data vary by up to factors of 4 and 1.3, respectively. These slip-rate variations appear to be restricted to time intervals of less than ~1700 to 2300 yr or ~5–8 times the mean recurrence interval of ~300 yr. For longer sample intervals the variability of earthquake parameters is averaged out by faulting processes and do not impact the rates.

6. Discussion

The variations in inferred SED and RI that contribute to temporal changes in slip rates for the Hope Fault could be associated with: (1) variable rupture lengths with earthquakes arresting at and propagating through geometry segment boundaries (Weldon et al., 2004; Khajavi et al., 2016), and (2) stress interactions between segments or nearby faults which promote or retard events on the Hurunui segment. The five segments on the Hope Fault are inferred to accrue slip during separate events. The segmentation model is consistent with paleoseismic studies along the fault (Cowan and McGlone, 1991; Langridge et al., 2003, 2013; Khajavi, 2015; Khajavi et al., 2016), but appears to be inconsistent with surface rupture during the only historical event on the fault, the 1888 M_w7.1 ± 0.1 Amuri earthquake (McKay, 1890) and possibly during an older earthquake event (i.e., 1479–1623 AD, Khajavi et al., 2016). The 1888 earthquake ruptured most of the Hope River segment and at least the eastern part of the Hurunui segment of the fault (Fig. 1), producing coseismic slips from 1.5 m to 2.6 m and a total rupture length of 44–70 km (Cowan, 1990; Langridge et al., 2013; Khajavi et al., 2016; this study). The Amuri earthquake indicates that Hope River-Hurunui segment boundary does not always coincide with rupture arrest. Based on the empirical rupture length and SED scaling relations of Wells and Coppersmith (1994), the range of SEDs estimated in this study could be produced by rupture of the Hurunui segment alone (length ~ 44 km and empirical SED 2 m), Hurunui and Hope River co-rupture (total length ~ 77 km and empirical SED 3.5 m) and rupture of the Taramakau, Hurunui and Hope River together (total length ~ 110 km and empirical SED 5 m). While these rupture scenarios have not been confirmed using paleoseismic data, the variations in SED suggest that characteristic surface-rupturing earthquakes may not apply on the Hurunui segment of the Hope Fault.

Variations in both SED and RI may be due to fault or segment interactions as has been widely postulated in numerous studies of paleoseismic data and numerical stress modelling (e.g., Weldon et al., 2004; Nicol et al., 2006; Dolan et al., 2007; Robinson et al., 2009; Ninis et al., 2013). Stress transfer and fault interactions involving the Hope Fault have been previously inferred from paleoseismic data (Langridge et al., 2013). Static stress modelling of fault systems shows that fault interactions can produce variations in the rates of strain release (i.e., earthquake slip and/or recurrence intervals) even when the fault strength, fault loading rates and stored stresses are approximately uniform (Ben-Zion, 1996; Robinson, 2004; Robinson et al., 2009). In these fault-interaction models, large-magnitude earthquakes stress and destress nearby active faults and may significantly advance and retard events. In this manner, SEDs and RIs can be expected to vary, particularly where faults are components of systems comprising many interacting elements (e.g., Nicol et al., 2006). Although such interactions have been widely inferred, in the case of the Hope Fault and neighbouring faults further work is required to examine the control of these interactions on the earthquake histories and slip rates.

7. Conclusions

We have estimated slip rates for ~230 to 13,000 yr time intervals on the Hurunui segment of the Hope Fault using geomorphic displacements measurement from LiDAR and radiocarbon dates. When averaged over time intervals of ≥2300 yr, or 5–8 times the mean earthquake recurrence interval of 266 ± 100 yr, the slip rates are approximately uniform (within the uncertainties) at 12.2 ± 2.4 mm/yr. At time intervals shorter than ~1700 yr, slip rates range by an order of magnitude from ~4 to 46.4 mm/yr. While some of this variability could be attributed to uncertainties in the displacement and age data, a significant component (> 50%) is due to temporal changes in SED (~2.2–4.6 m) and recurrence intervals (~128–560 yr) with the latter appearing to vary most. These variations reflect non-characteristic earthquake behaviour which may be due to changes in Hope fault loading arising from stress interactions with nearby faults and/or with different segments of the Hope Fault.

Acknowledgements

We wish to thank the NZ Natural Hazards Research Platform for funding LiDAR acquisition and the University of Canterbury (UC) the GNS Science (grant number 410UET21 Fault Geology), and the New Zealand Earthquake Commission (grant number E5713) for funding this research. The Department of Conservation and the owner of Poplars Station, Kevin Henderson, are thanked for permission to access the study area. We thank Amir Rezanejad for valuable field assistance. We wish to thank Liz Schermer and the anonymous reviewer for their very constructive comments which improved this work.

Appendix A. Supplementary data

Supplementary data to this article can be found online at https://doi.org/10.1016/j.tecto.2018.05.001. These data include interpreted LiDAR maps and the locations and detailed characteristics of the measured displacements data used in this article.

References

Alloway, B.V., Lowe, D.J., Barrell, D.J., Newnham, R.M., Almond, P.C., Augustinus, P.C., Bertler, N.A., Carter, L., Litchfield, N.J., McGlone, M.S., 2007. Towards a climate event stratigraphy for New Zealand over the past 30000 years (NZ-INTIMATE project). J. Quat. Sci. 22, 9–35.

Barrell, D.J.A., Townsend, D.B., 2012. General distribution and characteristics of active faults and folds in the Hurunui District, North Canterbury. GNS Science Consultancy Report 2012/113. (45 pp.).

Beauprêtre, S., Garambois, S., Manighetti, I., Malavieille, J., Sénéchal, G., Chatton, M., Davies, T., Larroque, C., Rousset, D., Cotte, N., Romano, C., 2012. Finding the buried record of past earthquakes with GPR-based palaeoseismology: a case study on the Hope fault, New Zealand. Geophys. J. Int. 189, 73–100.

Beavan, J., Tregoning, P., Bevis, M., Kato, T., Meertens, C., 2002. Motion and rigidity of the Pacific Plate and implications for plate boundary deformation. J. Geophys. Res. 107 (B10).

Ben-Zion, Y., 1996. Stress, slip, and earthquakes in models of complex single-fault systems incorporating brittle and creep deformations. J. Geophys. Res. 101, 5677–5706.

Berryman, K., Beanland, S., 1991. Variation in fault behaviour in different tectonic provinces of New Zealand. J. Struct. Geol. 13, 177–189.

Berryman, K.R., Beanland, S., Cooper, A.F., Cutten, H.N., Norris, R.J., Wood, P.R., 1992. The Alpine Fault, New Zealand: variation in Quaternary structural style and geomorphic expression. Annales Tectonicae 6, 126–163.

Clayton, L.S., 1965. Late Pleistocene Geology of the Waiau Valley, North Canterbury, New Zealand. University of Illinois, Urbana, pp. 91.

Clayton, L., 1968. Late Pleistocene glaciations of the Waiau valleys, north Canterbury. New Zeal. J. Geol. Geop. 11, 753–767.

Cowan, H.A., 1989. An Evaluation of the Late Quaternary Displacements and Seismic Hazard Associated With the Hope and Kakapou Faults, Amuri District, North Canterbury. Geological Sciences. University of Canterbury, Christchurch, pp. 239.

Cowan, H.A., 1990. Late Quaternary displacements on the Hope Fault at Glynn Wye, North Canterbury. N. Z. J. Geol. Geophys. 33, 285–293.

Cowan, H.A., McGlone, M.S., 1991. Late Holocene displacements and characteristic earthquakes on the Hope River segment of the Hope Fault, New Zealand. J. R. Soc. N. Z. 21, 373–384.

Cowie, P.A., Roberts, G.P., 2001. Constraining slip rates and spacings for active normal faults. J. Struct. Geol. 23, 1901–1915.

Cowie, P.A., Roberts, G.P., Bull, J.M., Visini, F., 2012. Relationships between fault geometry, slip rate variability and earthquake recurrence in extensional settings. Geophys. J. Int. 189, 143–160.

DeMets, C., Gordon, R.G., Argus, D.F., Stein, S., 1994. Effect of recent revisions to the geomagnetic reversal time scale on estimates of current plate motions. Geophys. Res. Lett. 21, 2191–2194.

DeMets, C., Gordon, R.G., Argus, D.F., 2010. Geologically current plate motions. Geophys. J. Int. 181, 1–80.

Dolan, J.F., Haravitch, B.D., 2014. How well do surface slip measurements track slip at depth in large strike-slip earthquakes? The importance of fault structural maturity in controlling on-fault slip versus off-fault surface deformation. Earth Planet. Sci. Lett. 388, 38–47.

Dolan, J.F., Bowman, D.D., Sammis, C.G., 2007. Long-range and long-term fault interactions in Southern California. Geology 35, 855–858.

Freund, R., 1971. The Hope Fault: a strike-slip fault in New Zealand. N. Z. Geol. Surv. Bull. 86 (49 pp.).

Hardy, E.F., Wellman, H.W., 1984. The Alpine, Wairau, and Hope Faults. University of Wellington Geology Department Publication, pp. 27.

Hartleb, R.D., Dolan, J.F., Akyüz, H.S., Yerli, B., 2003. A 2000-year-long Paleoseismologic record of earthquakes along the Central North Anatolian Fault, from trenches at Alayurt, Turkey. Bull. Seismol. Soc. Am. 93, 1935–1954.

Hartleb, R.D., Dolan, J.F., Kozaci, Ö., Akyüz, H.S., Seitz, G.G., 2006. A 2500-yr-long paleoseismologic record of large, infrequent earthquakes on the North Anatolian fault at Çukurçimen, Turkey. Geol. Soc. Am. Bull. 118, 823–840.

Hornblow, S., Quigley, M., Nicol, A., Van Dissen, R., Wang, N., 2014. Paleoseismology of the 2010 Mw 7.1 Darfield (Canterbury) earthquake source, Greendale Fault, New Zealand. Tectonophysics 637, 178–190.

Khajavi, N., 2015. Surface Rupture Morphology and Paleoseismology of the Western Hope Fault and Characteristics of Seismically-displaced Boulders in the Port Hills, South Island, New Zealand, Geological Sciences. University of Canterbury, Christchurch.

Khajavi, N., Quigley, M., Langridge, R.M., 2014. Influence of topography and basement depth on surface rupture morphology revealed from LiDAR and field mapping, Hope Fault, New Zealand. Tectonophysics 630, 265–284.

Khajavi, N., Langridge, R.M., Quigley, M.C., Smart, C., Rezanejad, A., Martín-González, F., 2016. Late Holocene rupture behavior and earthquake chronology on the Hope fault, New Zealand. Geol. Soc. Am. Bull. B31199, 31191.

Knuepfer, P.L.K., 1984. Tectonic Geomorphology and Present-day Tectonics of the Alpine Shear System, South Island, New Zealand (Neotectonics, Faults).

Knuepfer, P.L.K., 1988. Estimating ages of late Quaternary stream terraces from analysis of weathering rinds and soils. Geol. Soc. Am. Bull. 100, 1224–1236.

Knuepfer, P.L.K., 1992. Temporal variations in latest Quaternary slip across the Australian-Pacific plate boundary, northeastern South Island, New Zealand. Tectonics 11, 449–464.

Langridge, R.M., Berryman, K.R., 2005. Morphology and slip rate of the Hurunui section of the Hope Fault, South Island, New Zealand. New Zeal. J. Geol. Geop. 48, 43–57.

Langridge, R., Campbell, J., Hill, N., Pere, V., Pope, J., Pettinga, J., Estrada, B., Berryman, K., 2003. Paleoseismology and slip rate of the Conway Segment of the Hope Fault at Greenburn Stream, South Island, New Zealand. Ann. Geophys.-Italy 46, 1119–1140.

Langridge, R.M., Villamor, P., Basili, R., Almond, P., Martinez-Diaz, J.J., Canora, C., 2010. Revised slip rates for the Alpine fault at Inchbonnie: implications for plate boundary kinematics of South Island, New Zealand. Lithosphere 2, 139–152.

Langridge, R.M., Almond, P.C., Duncan, R.P., 2013. Timing of late Holocene paleoearthquakes on the Hurunui segment of the Hope fault: implications for plate boundary strain release through South Island, New Zealand. Geol. Soc. Am. Bull. 125, 756–775.

Lensen, G.J., 1962. Sheet 16- Kaikoura. In: Geological Map of New Zealand 1:250000. Department of Scientific and Industrial Research, Wellington, New Zealand.

Manighetti, I., Perrin, C., Dominguez, S., Garambois, S., Gaudemer, Y., Malavieille, J., Matteo, L., Delor, E., Vitard, C., Beauprêtre, S., 2015. Recovering paleoearthquake slip record in a highly dynamic alluvial and tectonic region (Hope fault, New Zealand) from airborne LiDAR. J. Geophys. Res. Solid Earth 120, 4484–4509.

Mason, D.P., Little, T.A., Van Dissen, R.J., 2006. Rates of active faulting during late Quaternary fluvial terrace formation at Saxton River, Awatere fault, New Zealand. Geol. Soc. Am. Bull. 118, 1431–1446.

McCalpin, J.P., 2009. Paleoseismology, 2 ed. Elsevier Science, Burlington.

McKay, A., 1890. On the earthquakes of September 1888 in the Amuri and Marlborough Districts of the South Island. In: New Zealand Geological Survey Report of Geological Explorations. 20. pp. 1–16.

McMorran, T.J., 1991. The Hope Fault at Hossack Station East of Hanmer Basin, North Canterbury. Geological Sciences. University of Canterbury, Christchurch, pp. 93.

Mouslopoulou, V., Walsh, J.J., Nicol, A., 2009. Fault displacement rates on a range of timescales. Earth Planet. Sci. Lett. 278, 186–197.

Nathan, S., Rattenbury, M.R., Suggate, R.P., 2002. Geology of the Greymouth area: scale 1:250,000. Lower Hutt: Institute of Geological & Nuclear Sciences. Institute of Geological & Nuclear Sciences 1:250,000 geological map 12. 58 p. + 1 folded map + 65 p.

Nicol, A., Van Dissen, R., 2002. Up-dip partitioning of displacement components on the oblique-slip Clarence Fault, New Zealand. J. Struct. Geol. 24, 1521–1535.

Nicol, A., Walsh, J., Berryman, K., Villamor, P., 2006. Interdependence of fault displacement rates and paleoearthquakes in an active rift. Geology 34, 865–868.

Nicol, A., Walsh, J., Mouslopoulou, V., Villamor, P., 2009. Earthquake histories and Holocene acceleration of fault displacement rates. Geology 37, 911–914.

Nicol, A., Langridge, R., Van Dissen, R., 2011. Wairau Fault Late Quaternary displacements and paleoearthquakes. In: Lee, J.M. (Ed.), Field Trip Guides, Geosciences 2011 Conference, Nelson, New Zealand. Geoscience Society of New Zealand Miscellaneous

Publication 130B, (33 pp.).
Nicol, A., Robinson, R., Van Dissen, R.J., Harvison, A., 2016. Variability of recurrence interval and single-event slip for surface-rupturing earthquakes in New Zealand. N. Z. J. Geol. Geophys. 59, 97–116.
Nicol, A., Seebeck, H., Wallace, L., 2017. Quaternary tectonics of New Zealand. In: Schulmeister, J. (Ed.), Atlantis Advances in Quaternary Science: Landscape and Quaternary Environmental Change in New Zealand, Atlantis Press, pp. 1–34. http://dx.doi.org/10.2991/978-94-6239-237-3_1.
Ninis, D., Little, T.A., Van Dissen, R.J., Litchfield, N.J., Smith, E.G., Wang, N., Rieser, U., Henderson, C.M., 2013. Slip rate on the Wellington fault, New Zealand, during the late Quaternary: evidence for variable slip during the Holocene. Bull. Seismol. Soc. Am. 103, 559–579.
Norris, R.J., Cooper, A.F., 2001. Late Quaternary slip rates and slip partitioning on the Alpine Fault, New Zealand. J. Struct. Geol. 23, 507–520.
Oskin, M., Perg, L., Shelef, E., Strane, M., Gurney, E., Singer, B., Zhang, X., 2008. Elevated shear zone loading rate during an earthquake cluster in eastern California. Geology 36, 507–510.
Parsons, T., 2008. Monte Carlo method for determining earthquake recurrence parameters from short paleoseismic catalogs: example calculations for California. J. Geophys. Res. Solid Earth 113 (n/a-n/a).
Polonia, A., Gasperini, L., Amorosi, A., Bonatti, E., Bortoluzzi, G., Çagatay, N., Capotondi, L., Cormier, M.H., Gorur, N., McHugh, C., Seeber, L., 2004. Holocene slip rate of the North Anatolian Fault beneath the Sea of Marmara. Earth Planet. Sci. Lett. 227, 411–426.
Quigley, M., Van Dissen, R., Litchfield, N., Villamor, P., Duffy, B., Barrell, D., Furlong, K., Stahl, T., Bilderback, E., Noble, D., 2012. Surface rupture during the 2010 Mw 7.1 Darfield (Canterbury) earthquake: implications for fault rupture dynamics and seismic-hazard analysis. Geology 40, 55–58.
Rattenbury, M.S., Townsend, D., Johnston, M.R., 2006. Geology of the Kaikoura area: scale 1:250,000 geological map. Lower Hutt: GNS Science. Institute of Geological & Nuclear Sciences 1:250,000 geological map 13. 70 p. + 1 folded map.
Rittase, W.M., Kirby, E., McDonald, E., Walker, J.D., Gosse, J., Spencer, J.Q., Herrs, A., 2014. Temporal variations in Holocene slip rate along the central Garlock fault, Pilot Knob Valley, California. Lithosphere 6, 48–58.
Robinson, R., 2004. Potential earthquake triggering in a complex fault network: the northern South Island, New Zealand. Geophys. J. Int. 159, 734–748.
Robinson, R., Nicol, A., Walsh, J., Villamor, P., 2009. Features of earthquake occurrence in a complex normal fault network: results from a synthetic seismicity model of the Taupo Rift, New Zealand. J. Geophys. Res. Solid Earth 114.
Rockwell, T.K., Klinger, Y., 2013. Surface rupture and slip distribution of the 1940 Imperial Valley earthquake, Imperial Fault, Southern California: implications for rupture segmentation and dynamics. Bull. Seismol. Soc. Am. 103, 629–640.
Scharer, K.M., Weldon, R.J., Fumal, T.E., Biasi, G.P., 2007. Paleoearthquakes on the southern San Andreas Fault, Wrightwood, California, 3000 to 1500 B.C.: a new method for evaluating paleoseismic evidence and earthquake horizons. Bull. Seismol. Soc. Am. 97, 1054–1093.
Scharer, K.M., Salisbury, J.B., Arrowsmith, J.R., Rockwell, T.K., 2014. Southern San Andreas fault evaluation field activity: approaches to measuring small geomorphic offsets—challenges and recommendations for active fault studies. Seismol. Res. Lett. 85, 68–76.
Suggate, R.P., 1965. Late Pleistocene geology of the Northern Part of the South Island, New Zealand. New Zealand Dept. of Scientific and Industrial Research.
Suggate, R.P., Stevens, G.R., Te Punga, M.T., 1978. The Geology of New Zealand. Government Printer, Wellington (2 vols., 820 pp.).
Thompson, S.C., Weldon, R.J., Rubin, C.M., Abdrakhmatov, K., Molnar, P., Berger, G.W., 2002. Late Quaternary slip rates across the central Tien Shan, Kyrgyzstan, central Asia. J. Geophys. Res. Solid Earth 107 (ETG 7-1–ETG 7-32).
Van Dissen, R., 1989. Late Quaternary Faulting in the Kaikoura Region, Southeastern Marlborough, New Zealand. Unpublished MS Thesis. Oregon State University, USA (72 pp.).
Van Dissen, R., Nicol, A., 2009. Mid-late Holocene paleoseismicity of the eastern Clarence Fault, Marlborough, New Zealand. New Zeal. J. Geol. Geoph. 52, 195–208.
Van Dissen, R., Yeats, R.S., 1991. Hope Fault, Jordan Thrust, and uplift of the Seaward Kaikoura Range, New Zealand. Geology 19, 393–396.
Wallace, L.M., Beavan, J., McCaffrey, R., Berryman, K., Denys, P., 2007. Balancing the plate motion budget in the South Island, New Zealand using GPS, geological and seismological datas. Geophys. J. Int. 168, 332–352.
Wallace, L.M., Barnes, P., Beavan, J., Van Dissen, R., Litchfield, N., Mountjoy, J., Langridge, R., Lamarche, G., Pondard, N., 2012. The kinematics of a transition from subduction to strike-slip: an example from the central New Zealand plate boundary. J. Geophys. Res. B: Solid Earth 117.
Weldon, R.J., Sieh, K.E., 1985. Holocene rate of slip and tentative recurrence interval for large earthquakes on the San Andreas Fault, Cajon Pass, southern California. Geol. Soc. Am. Bull. 96, 793–812.
Weldon, R., Scharer, K., Fumal, T., Biasi, G., 2004. Wrightwood and the earthquake cycle: what a long recurrence record tells us about how faults work. GSA Today 14, 4–10.
Wellman, H.W., 1985. Rate of Dextral Faulting in the Central Part of New Zealand From Weathering Rind Ages. Unpublished Draft Report. Dept. of Geology, Research School of Earth Sciences, V.U.W., Wellington.
Wells, D.L., Coppersmith, K.J., 1994. New empirical relationships among magnitude, rupture length, rupture width, rupture area, and surface displacement. Bull. Seismol. Soc. Am. 84, 974–1002.
Wood, R.A., Pettinga, J.R., Bannister, S., Lamarche, G., McMorran, T.J., 1994. Structure of the Hanmer strike-slip basin, Hope Fault, New Zealand. Bull. Geol. Soc. Am. 106, 1459–1473.
Yang, J.S., 1991. The Kakapo Fault — a major active dextral fault in the central North Canterbury - Buller regions of New Zealand. New Zeal. J. Geol. Geop. 34, 137–143.
Zachariasen, J., Berryman, K., Langridge, R., Prentice, C., Rymer, M., Stirling, M., Villamor, P., 2006. Timing of late Holocene surface rupture of the Wairau Fault, Marlborough, New Zealand. New Zeal. J. Geol. Geop. 49, 159–174.
Zielke, O., Arrowsmith, J.R., Ludwig, L.G., Akçiz, S.O., 2010. Slip in the 1857 and earlier large earthquakes along the Carrizo Plain, San Andreas Fault. Science 327, 1119–1122.
Zielke, O., Arrowsmith, J.R., Ludwig, L.G., Akciz, S.O., 2012. High-resolution topography-derived offsets along the 1857 Fort Tejon earthquake rupture trace, San Andreas Fault. Bull. Seismol. Soc. Am. 102, 1135–1154.
Zielke, O., Klinger, Y., Arrowsmith, J.R., 2015. Fault slip and earthquake recurrence along strike-slip faults — contributions of high-resolution geomorphic data. Tectonophysics 638, 43–62.